

Finite element analysis of transmission of leaky Rayleigh waves at the extremity of a fluid-loaded thick plate

Ebrahim Lamkanfi^{a)}

Department of Mechanical Construction and Production, Ghent University, Sint-Pietersnieuwstraat 41, 9000 Ghent, Belgium

Nico F. Declercq

Georgia Institute of Technology, George W. Woodruff School of Mechanical Engineering, 801 Ferst Drive, Atlanta, Georgia 30332-0405 and Georgia Tech Lorraine, UMI Georgia Tech—CNRS 2958, 2 rue Marconi, 57070 Metz, France

Wim Van Paepelgem and Joris Degrieck

Department of Mechanical Construction and Production, Ghent University, Sint-Pietersnieuwstraat 41, 9000 Ghent, Belgium

(Received 16 January 2007; accepted 5 April 2007; published online 6 June 2007)

A numerical study based on finite element simulations reveals the experimentally indicated fact [N. F. Declercq *et al.*, *J. Appl. Phys.* **96**, 5836 (2004)] that leaky Rayleigh waves propagating along the horizontal surface of a thick fluid-loaded solid plate are transmitted around the corner of the solid plate. The mentioned experiments are based on the so-called Schoch effect, accompanied by the presence of a null strip in the reflected part of the beam, and phenomena occurring when the incident beam, generating the effect, approaches the edge of the solid plate. The referred experiments indicate that leaky Rayleigh waves are generated around the corner of the plate, but the experimental evidence is not fully conclusive whether the effect is caused merely by incident Rayleigh waves on the upper surface or by scattering effects when the incident beam interacts with the corner. The current study first confirms the reported experiments by means of the finite element method and then proves that the assumption made in the referred paper about Rayleigh waves, being primarily stimulated by the edge of an incident bounded beam rather than the middle, is correct. Ultimately the model is applied to study leaky Rayleigh waves separately from the incident and reflected bounded beams. It is shown that the Rayleigh waves themselves are the physical origin of the transmission of Rayleigh waves rather than scattering effects caused by the incident bounded beam.

© 2007 American Institute of Physics. [DOI: [10.1063/1.2738407](https://doi.org/10.1063/1.2738407)]

I. INTRODUCTION

Rayleigh waves are well-known elliptically polarized surface waves on the surface of a solid. They have been a subject of study in both geology and in ultrasonics. When the surface is covered by a liquid, such as when a thick solid plate is immersed in water, Rayleigh waves leak energy into the liquid and are called leaky Rayleigh waves. Leaky Rayleigh waves are particularly useful for nondestructive purposes because they enable the detection of surface and subsurface defects and they can be generated by means of an incident ultrasonic bounded beam. The propagation of sound is governed by continuum mechanics and can be sufficiently approximated by means of the finite element method (FEM) if the smallest element size is much smaller than the accompanied wavelengths involved. In this paper we aim at understanding the behavior of leaky Rayleigh waves when they reach the edge of a thick plate. Furthermore we try to reveal whether Rayleigh waves actually propagate around the corner. Our research is triggered by an earlier paper¹ that shows experimentally how a bounded beam, incident at the Rayleigh angle on a solid plate, interacts with the edge of that

plate. The experiments show that leaky Rayleigh waves are generated along the vertical edge of the plate. Still, even though assumed and more or less put to evidence, no indisputable and conclusive confirmation is shown as to whether these vertical leaky Rayleigh waves are really generated by incident leaky Rayleigh waves or are merely a consequence of scattering of the incident beam at the corner of the plate. In Ref. 1 there is also an experimental indication that leaky Rayleigh waves are primarily stimulated by the edge of the incident beam rather than the middle. Numerical simulations, based on FEM, must solve these mysteries.

First, we explain very briefly what a finite element method is and how it is used to solve the coupled acoustic-structural interaction. Next, we show how the Schoch effect^{2–9} accompanied by a null strip¹⁰ can be simulated at a fluid-solid interface of infinite extent. Consequently we move the ultrasound beam to the extremity of the solid plate. In this way we try to observe how certain edge effects that occur under the Rayleigh angle also can be obtained by means of FEM. Next, an additional study reveals which part of the incident beam is the most effective in stimulating the generation of Rayleigh waves. Finally, we answer the question whether the Rayleigh waves do actually propagate around the corner of the solid plate or not.

^{a)}Author to whom correspondence should be addressed; electronic mail: ebrahim.lamkanfi@lid.kiviv.be

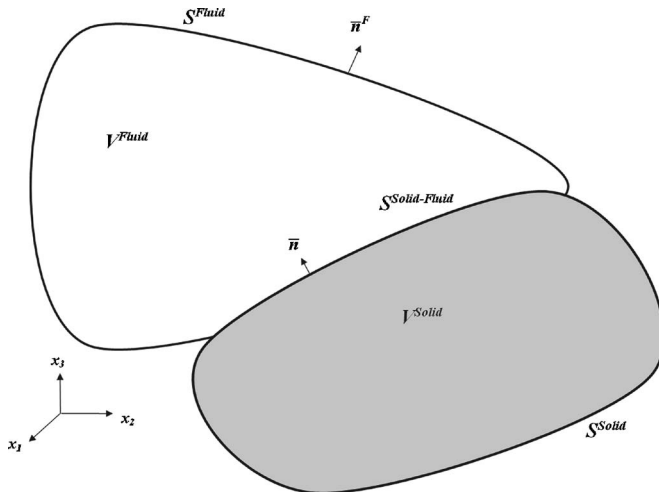


FIG. 1. Solid medium V^{solid} in contact with a fluid medium V^{fluid} with $S^{\text{solid-fluid}}$ as the interaction surface.

II. FINITE ELEMENT FORMULATION

During the past two decades, finite element methods have extensively been used in many engineering fields with great success. These methods represent a general class of techniques for the approximate solution of partial differential equations. Apart from mechanical,^{11–17} thermal,^{18–22} and electrical problems,^{23–26} also acoustic^{27–32} and even coupled acoustic-structural problems^{33–37} can be handled with these methods. In the finite element formulation of acoustic-structural problems, the necessary partial differential equations (PDE's) to describe the coupled problem can be derived from the conservation law of linear momentum. In the next paragraph the necessary equations for solving the acoustic-structural problem will be given. Consider Fig. 1 where a solid volume $V^{\text{solid}}=V^S$ with boundary surface $S^{\text{solid}}=S^S$ is in contact with a fluid medium $V^{\text{fluid}}=V^F$ having a boundary surface $S^{\text{fluid}}=S^F$. The solid is described by the differential equation of motion for a continuum volume assuming small deformations and the fluid by the acoustic wave equation. Coupling conditions at the boundary surface $S^{\text{solid-fluid}}=S^{\text{S-F}}$ between the structural and fluid domain ensure the continuity in displacement and pressure between the two domains.

A. Acoustic formulation

In each of the three orthogonal directions x_i ($i=1,\dots,3$) (Fig. 1) the governing equations for small motions of the fluid medium V^F , which is assumed to be nonviscous, rotational-free, compressible, and with no velocity-dependent momentum loss, can be written as

$$-\rho_F \frac{\partial^2 u_i^F}{\partial t^2} + \frac{\partial p}{\partial x_i} = 0 \quad \text{on } V^F. \quad (1)$$

The constitutive behavior of the fluid which relates the pressure in the fluid to the spatial derivative of the displacement can be described as

$$p = -B_F \sum_{i=1}^3 \frac{\partial u_i^F}{\partial x_i}. \quad (2)$$

Taking the divergence of Eq. (1) and substituting Eq. (2), the acoustic wave equation is found,

$$-\frac{\rho_F}{B_F} \frac{\partial^2 p}{\partial t^2} + \nabla^2 p = 0, \quad (3)$$

where $\nabla^2 = \partial^2 / \partial x_1^2 + \partial^2 / \partial x_2^2 + \partial^2 / \partial x_3^2$ is the Laplace operator.

For solving the partial differential Eq. (3), some necessary conditions have to be satisfied on the boundary surface S^F , before a unique solution can be obtained. On a part of this boundary, $S_{\tilde{u}}^F$, where the acceleration is specified, a special form of Eq. (1) has to be fulfilled,

$$\frac{\partial p}{\partial n_i^F} = -\rho_F \frac{\partial^2 u_{n,i}^F}{\partial t^2} \quad \text{on } S_{\tilde{u}}^F. \quad (4)$$

For the part S_p^F of the boundary surface S^F , the pressure field p has to fulfill the prescribed values that are denoted with a tilde ($\tilde{\cdot}$),

$$p = \tilde{p} \quad \text{on } S_p^F. \quad (5)$$

In the equations above $p=p(x_1, x_2, x_3, t)$ is the scalar pressure field relative to the hydrostatic pressure, $\bar{x}=(x_1, x_2, x_3, t)$ the spatial coordinate vector, t is the time, ρ_F is the mass density of the fluid, $\bar{u}^F=(u_1^F, u_2^F, u_3^F, t)$ is the fluid particle displacement vector, B_F is the bulk modulus of the fluid, $\bar{n}^F=(n_1^F, n_2^F, n_3^F)$ is the unit normal vector on the fluid surface, $\partial^2 u_{n,i}^F / \partial t^2$ is the i th ($i=1\dots 3$) component of the acceleration vector $\partial^2 \bar{u}_n^F / \partial t^2$ on the fluid boundary in the direction of the normal to that boundary.

To derive the finite element formulation for the acoustic domain, Eq. (3) is multiplied by a virtual pressure field $\delta p = \delta p(x_1, x_2, x_3, t)$ that is defined as a continuous scalar field on V^F and S^F . After taking the integration over the specified domains and the application of the Gauss' theorem, the weak formulation of the acoustical problem is achieved as follows:

$$-\int \int \int_{V^F} (\delta p) \frac{\rho_F}{B_F} \frac{\partial^2 p}{\partial t^2} dV + \int \int \int_{V^F} \nabla(\delta p) \nabla p dV \\ + \int \int_{S^F} (\delta p) \rho_F \frac{\partial^2 \bar{u}_n^F}{\partial t^2} dS = 0. \quad (6)$$

To obtain the discretized form of Eq. (6), the domain V^F has to be divided into m finite elements, where the pressure field is approximated. After the substitution of these approximations and the elimination of the virtual pressure field in Eq. (6), the acoustic wave equation in its discretized form becomes

$$M^F \ddot{P}(t) + K^F P(t) = -R^F(t), \quad (7)$$

with

$$M^F = \sum_1^m \frac{\rho_F}{B_F} \int \int \int_{V^{Fe}} Q^T Q dV^e, \quad (8)$$

$$K^F = \sum_1^m \int \int \int_{V^F} F^T F dV^e, \quad (9)$$

$$R^F(t) = \sum_1^m \rho_F \int \int_{S^F} Q^T \frac{\partial^2 \bar{u}_n^F}{\partial t^2} dS^e, \quad (10)$$

where Q is the row vector of interpolation functions, $P(t)$ is the vector of the pressure in the nodes at time t , F is the matrix of spatial derivatives of the interpolation functions for the fluid, M^F is referred to as the fluid mass matrix, K^F is the fluid stiffness matrix, and R^F is the fluid external force vector.

B. Structural formulation

In each point of an arbitrary continuum body V^S , with surface S^S (Fig. 1), the governing partial differential equation of motion can be written as

$$\frac{\partial \sigma_{ij}}{\partial x_j} - \rho_S \frac{\partial^2 u_i^S}{\partial t^2} + f_i^S = 0 \quad \text{on } V^S. \quad (11)$$

In this equation σ_{ij} is the Cauchy stress tensor, x_j is the j th component ($j=1 \dots 3$) of the spatial vector \bar{x} , ρ_S is the density of the solid medium (assumed to be constant), u_i^S is the i th component ($i=1 \dots 3$) of the displacement vector \bar{u}^S , t is the time, and f_i^S is the i th component ($i=1 \dots 3$) of the body force \bar{f}^S acting on the solid medium V^S .

In the case of small strains and deformations, which is justified in the case of the incidence of an acoustical wave on a structural part, the kinematic relationship between the displacements and the strains in that body can be presented as

$$\varepsilon_{ij} = \frac{1}{2} \left(\frac{\partial u_i^S}{\partial x_j} + \frac{\partial u_j^S}{\partial x_i} \right), \quad (12)$$

where ε_{ij} represents the Green-Lagrange strain tensor. The constitutive model describing the relation between the stresses and strains for an isotropic material, e.g., aluminum, can be described as

$$\sigma_{ij} = \frac{E}{1+\nu} \left(\varepsilon_{ij} + \delta_{ij} \frac{\nu}{1-2\nu} I_1 \right), \quad (13)$$

with

$$I_1 = \varepsilon_{11} + \varepsilon_{22} + \varepsilon_{33}. \quad (14)$$

The solution of the partial differential equation found by combining Eqs. (11)–(13) can only be found if a set of boundary conditions is specified and fulfilled on the boundary surface S^S . Two boundary conditions are taken into account:

$$u_i^S = \tilde{u}_i^S \quad \text{on } S_U^S, \quad (15)$$

$$\sum_{j=1}^3 \sigma_{ij} n_j = \phi_i^S \quad \text{on } S_T^S \text{ for } (i=1 \dots 3). \quad (16)$$

In Eq. (15) the tilde (~) means that the displacement \tilde{u}_i^S is specified on S_U^S . In the other equations n_j is the j th component ($j=1 \dots 3$) of unit normal vector \bar{n} on the surface S^S , ϕ_i^S

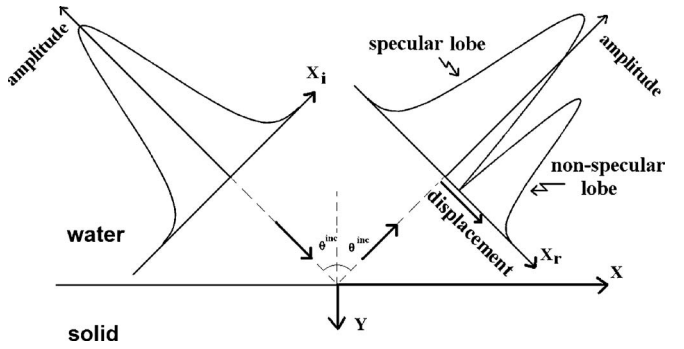


FIG. 2. Schematic visualization of the Schoch effect. Picture taken from Ref. 1.

is the i th component of the traction vector $\bar{\phi}^S$, E is Young's modulus, ν Poisson's ratio, δ_{ij} is Kronecker's delta, S_T^S is the part of the boundary where external traction is specified, and S_U^S is the part of the boundary where the displacement is specified.

If we interpret δu_i^S as the i th component ($i=1 \dots 3$) of a virtual displacement vector $\delta \bar{u}^S$ and $\delta \varepsilon_{ij}^S$ as the corresponding virtual strain and if we assume that no body forces exist, then the virtual work done by the external loadings and the internal stresses integrated over the entire body V^S can be written in the following way:

$$-\int \int \int_{V^S} \rho_S \frac{\partial^2 u_i^S}{\partial t^2} \delta u_i^S dV + \int \int_{S^S} \phi_i^S \delta u_i^S dS - \int \int \int_{V^S} \sigma_{ij} \delta \varepsilon_{ij}^S dV = 0 \quad (17)$$

with

$$\delta \varepsilon_{ij}^S = \frac{1}{2} \left(\frac{\partial \delta u_i^S}{\partial x_j} + \frac{\partial \delta u_j^S}{\partial x_i} \right). \quad (18)$$

It has to be observed that the virtual displacement vector satisfies all the boundary conditions defined on the surface S^S . Writing the tensors ε_{ij} and σ_{ij} in their respective matrix forms ε^S and σ^S , Eq. (17) can be transformed in

$$-\int \int \int_{V^S} (\delta \bar{u}^S)^T \rho_S \frac{\partial^2 \bar{u}^S}{\partial t^2} dV + \int \int_{S^S} (\delta \bar{u}^S)^T \bar{\phi}^S dS - \int \int \int_{V^S} (\delta \varepsilon^S)^T \sigma^S dV = 0. \quad (19)$$

Dividing the domain V^S into n finite elements, in which for each of them an approximation is introduced for the displacement vector

$$\bar{u}^S(\bar{x}, t) = H(\bar{x}) \bar{u}^e(t) \quad (20)$$

and for the virtual displacement vector

$$\delta \bar{u}^S(\bar{x}, t) = H(\bar{x}) \delta \bar{u}^e(t), \quad (21)$$

gives the discretized equation of motion after elimination of the virtual displacement field vector in Eq. (19) as follows:

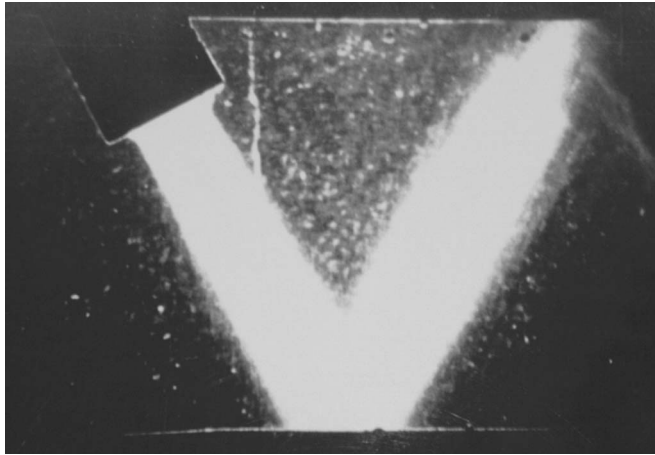


FIG. 3. Laboratory experiment (schlieren picture) of a 4 MHz Gaussian beam with 25° as angle of incidence.

$$M^S \ddot{U}(t) + R^{\text{int}}(t) = R^{\text{ext}}(t) \quad (22)$$

with

$$M^S = \sum_1^n \int \int \int_{V^{Se}} \rho_S H^T H dV^e, \quad (23)$$

$$R^{\text{int}}(t) = \sum_1^n \int \int \int_{V^{Se}} B^T \sigma^S dV^e, \quad (24)$$

$$R^{\text{ext}}(t) = \sum_1^n \int \int_{S^e} H^T \bar{\phi}^S dS^e. \quad (25)$$

In Eqs. (22)–(25) M^S is the structural mass matrix, $\ddot{U}(t)$ is the nodal acceleration vector, $R^{\text{int}}(t)$ is the internal force vector, $R^{\text{ext}}(t)$ is the external force vector, $H(\bar{x})$ or H is the matrix containing the interpolation functions for an element, and $B(\bar{x})$ or B is the matrix containing the spatial derivatives of the interpolation functions.

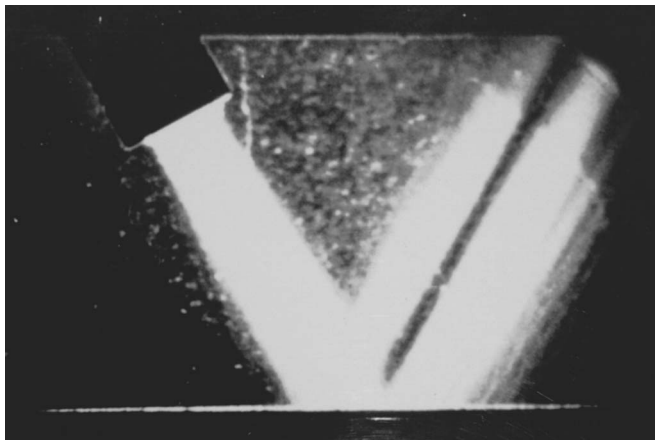


FIG. 4. Laboratory experiment (schlieren picture) of a 4 MHz Gaussian beam with 31° as angle of incidence.

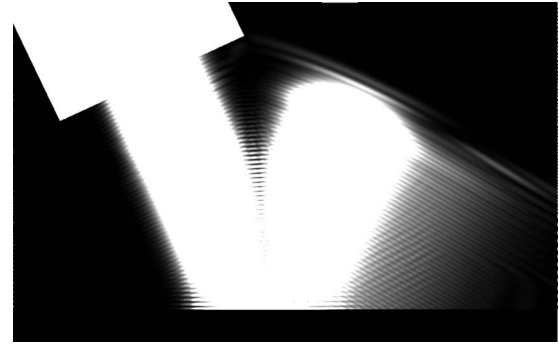


FIG. 5. An incident 4 MHz ultrasonic Gaussian beam on an aluminum plate under an angle of 25°.

C. The coupled structural-acoustical partial differential equations

By gathering the necessary Eqs. (7)–(10) and (22)–(25) that characterize the coupled model, a system of partial differential equations is formed. The boundary condition that describes the interaction between the two media enforces the acceleration of the fluid at the interface to be the same as the acceleration of the solid at that interface. It gives a proportional relation between a pressure at the interface and the corresponding structural acceleration. In this way the physical condition expressed by the classical impedance equations between two media is fulfilled at the interface.

Defining S^{S-F} as the structural-fluid interface (Fig. 1), the discretized finite element equations for the coupled fluid-structure system are expressed as

$$M^F \ddot{P}(t) + K^F P(t) = -R^F(t) - \rho_F I^T \ddot{U}(t) \quad (26)$$

and

$$M^S \ddot{U}(t) + R^{\text{int}}(t) = R^{\text{ext}}(t) + I P(t). \quad (27)$$

Discretizing the interaction surface S^{S-F} into r elements, the expression for the global interaction matrix I is written as

$$I = \sum_1^r \int \int_{S^{Se-Fe}} \rho_F H^T \bar{n}^F H dS^e. \quad (28)$$

By solving this system of equations in every node and during a certain time interval, in the case of a direct integration scheme, a distribution of the acoustic pressure, the displacement, and the accelerations of the nodes at the fluid-solid

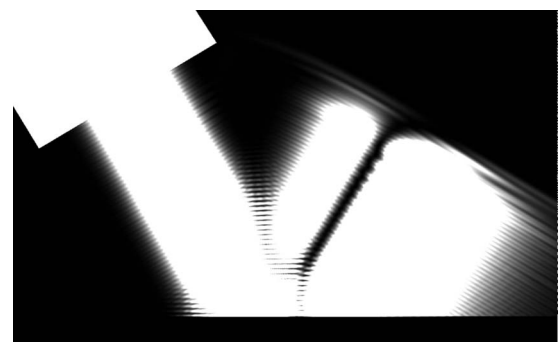


FIG. 6. Schoch effect: formation of specular lobes by an incident 4 MHz ultrasonic Gaussian beam on an aluminum plate under the Rayleigh angle.

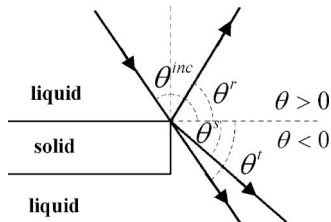


FIG. 7. Definition of the different angles θ^{inc} , θ^r , θ^s , and θ^t . The angles are measured from the horizontal axis left from the plate. The positive angles are anticlockwise, whereas the negative angles are clockwise. Picture taken from Ref. 1.

interface can be obtained. Because of the increase of computing power, the finite element method has become a very attractive way to solve these coupled acoustic-structural problems. In what follows, it is used to obtain a better understanding of the acoustic wave propagation of Rayleigh waves at the extremity of a fluid-loaded thick solid plate. But before handling this problem, we will prove that this method is suitable to describe a well-known basic ultrasonic phenomenon lying behind the extremity problem, i.e., the simulation of the Schoch effect.

III. SCHOCH EFFECT

The Schoch effect arises when an ultrasonic beam is incident at the Rayleigh angle (measured from the normal to the liquid/solid interface); then the reflected beam at the interface surface, in most cases, shows up as two lobes (Fig. 2) separated by a zone with no pressure distribution. The first lobe is generally called the specular lobe, and the second one is usually referred to as the nonspecular lobe. The existence of the nonspecular lobe is a consequence of the generation of leaky Rayleigh waves. Its exact origin is believed to be the interaction of the leakage field with the specular sound field resulting in a null strip where the specular lobe is in antiphase with the leakage field. At angles different from the Rayleigh angle, the reflected beam will not split up. The presence of a null strip was reported by Neubauer and Dragonet.¹⁰ The specular lobe is also shifted in space. The shift of position is referred to as the Schoch effect.^{38,39}

In the experiment of Fig. 3, a relatively large aluminum plate (large enough to make sure that no edge effects are involved) is used with the following material properties: Young's modulus ($E=7.55 \times 10^{10} \text{ N/m}^2$), Poisson's ratio ($\nu=1/3$), and density ($\rho_S=2700 \text{ kg/m}^3$). This plate is immersed in water, which will act as the propagation medium

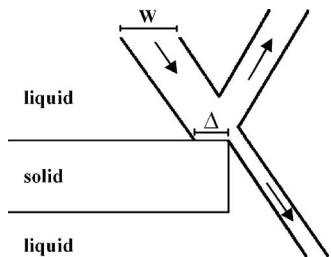


FIG. 8. Definition of Δ : the distance between the first beam edge and the plate edge and W : the horizontal physical width of the beam. Picture taken from Ref. 1.

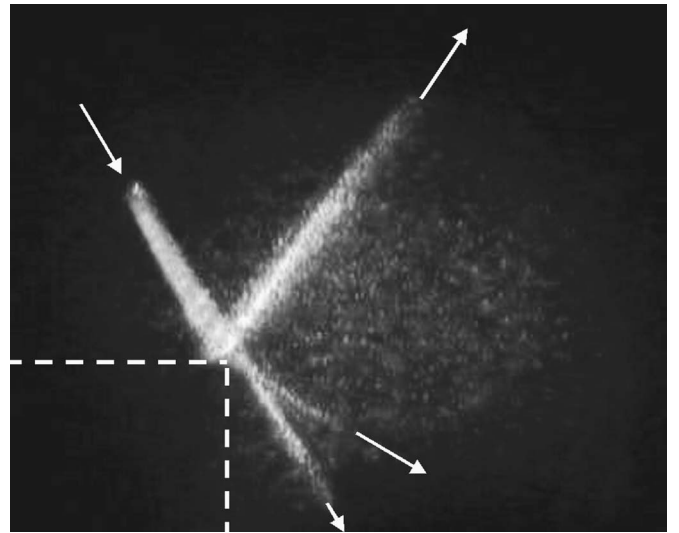


FIG. 9. Incidence of a 6 MHz, 6-mm-wide bounded beam on aluminum. $W \approx 7 \text{ mm}$ and $\Delta \approx 0.6W$ (schlieren picture). The dashed lines show where the plate is situated in the experiment. The arrows show the sound propagation direction. Picture taken from Ref. 1.

for a 4 MHz ultrasonic beam with a Gaussian width of 15 mm. The angle of the incident beam in Fig. 3 is slightly different from the critical Rayleigh angle. In this case we can see that the beam just reflects on the aluminum surface without splitting up. In a second experiment (Fig. 4), where the beam radiates under an angle of 31°, the Schoch effect, as explained above, unfolds. Similar effects are not visible at other angles, in correspondence with experiments as in Fig. 2. Before trying to simulate more complex ultrasonic phenomena, a reproduction of this split phenomenon of the ultrasonic beam is desirable using the finite element method. To do this, the commercial finite element package ABAQUS™ 6.5-1 is used to implement a model for the laboratory experiments. For the water medium two dimensional four-node linear, quadrilateral acoustic elements, with the acoustic pressure p as the only degree of freedom, have been used and for the solid medium four-node continuum bilinear plane strain quadrilateral elements have been chosen. The interaction between these two media is modeled using a tie constraint which enforces the coupled calculations. All other boundaries of the fluid medium as well as those of the solid medium are considered as purely reflective boundaries. In this way a numerical model is constructed to simulate the experi-

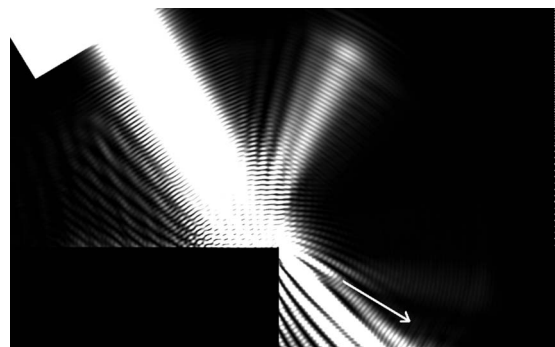


FIG. 10. Simulation of an incident 6 MHz, 6-mm-wide Gaussian beam at the extremity of an aluminum plate.

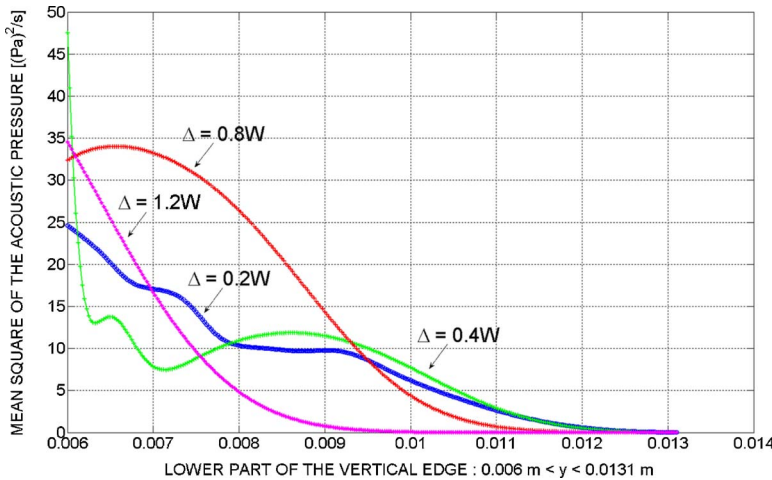


FIG. 11. (Color online) The mean square of the acoustic pressure in function of the distance along the vertical edge: $0.006\text{m} < y < 0.0131\text{m}$.

ments shown in Figs. 3 and 4. The outcome of the calculations can be found in Figs. 5 and 6, where, respectively, a 25° and a 31° incident beam is used. In these figures the square of the pressure amplitude, which is proportional to the sound intensity, is shown which makes a comparison with the schlieren pictures of Figs. 3 and 4 possible. In Fig. 5, the beam reflects on the aluminum surface in correspondence with the experiment shown in Fig. 3. In Fig. 6 it is clear that the beam splits into two lobes under the Rayleigh angle as expected.

IV. EXTREMITY OF A SOLID PLATE

In this paragraph we will take a closer look at the edge effects that occur when the Gaussian ultrasonic beam is moved to the extremity of the aluminum plate. A schematic representation of this experiment is shown in Fig. 7 where the angles represent the wave propagation direction of the different beams observed during the experiment: θ^{inc} is the incident angle of the Gaussian ultrasonic beam measured from the vertical on the solid-fluid interface, the reflected beam makes an angle θ' with the horizontal on the right-hand side of the plate, θ'' is the angle between the same horizontal and the incident beam that propagates through the fluid medium without being disturbed by the solid surface, and θ' is the angle of an additional observed beam with the horizontal

of which the existence will be explained in the succeeding paragraph. As one can see in Fig. 8 the symbol W represents the horizontal physical width of the Gaussian beam and Δ is the distance between the first beam edge and the edge of the plate. It is known that when a beam is incident on the edge of a plate under the Rayleigh angle, a part of the beam will be reflected, the other part will propagate in an undisturbed manner, and a third beam will make the Rayleigh angle with the horizontal (Fig. 7). Declercq *et al.*¹ have extensively described this wave generation along the vertical edge of the solid plate. However, two assumptions were made concerning the generation of Rayleigh waves. In a first one it was stated that the observed beam generation on the vertical edge was due to the propagation of the leaky Rayleigh waves around the corner (Fig. 9) and in a second one it was said that the outer parts of the Gaussian beam were mainly responsible for the generation of the Rayleigh waves. The explanation given for this last assumption was that the edge of the Gaussian beam has a profile that is quite similar to that of an inhomogeneous wave, such as a bounded beam with an exponentially varying amplitude profile (Fig. 7 of Ref. 1), which should be more suitable to stimulate the generation of the Rayleigh waves. Because it is difficult to prove both assumptions analytically by using an extension of the radia-

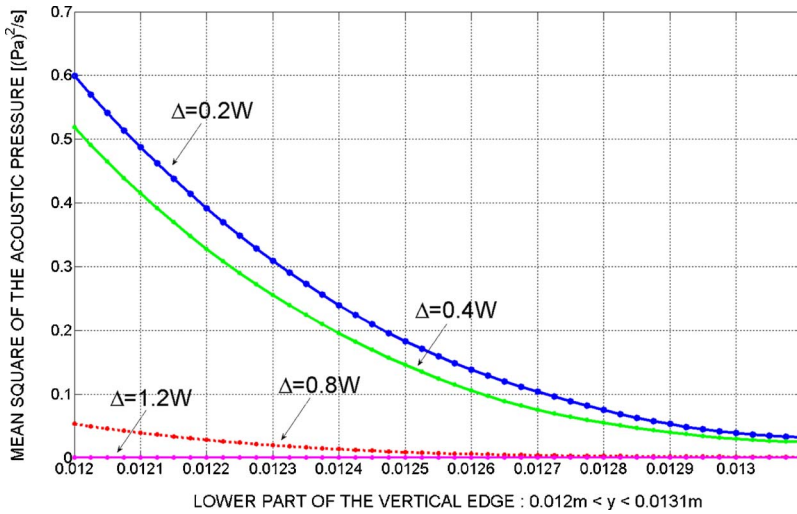


FIG. 12. (Color online) The mean square of the acoustic pressure in function of the distance along the lower part of the vertical edge: $0.012\text{m} < y < 0.0131\text{m}$.

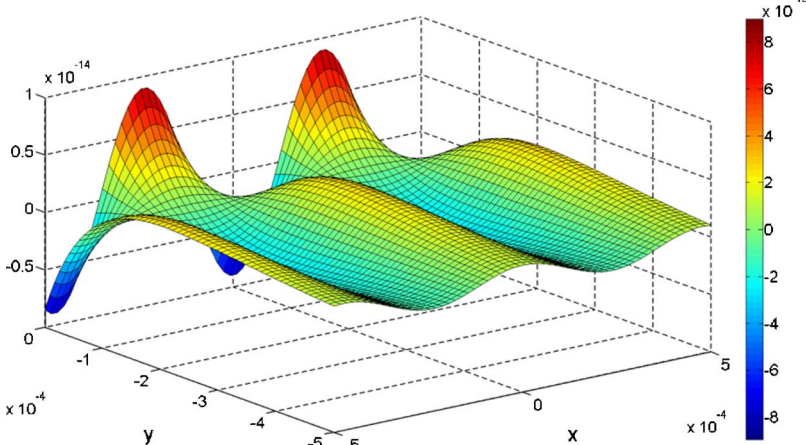
TABLE I. Values for the constants in the equations of motion of a Rayleigh wave in an aluminum plate immersed in water.

Variable	Real part [-]	Imaginary part [-]
α	$1.325\ 14 \times 10^4$...
β	$2.175\ 40 \times 10^4$...
χ	...	$-1.187\ 93 \times 10^4$
ε	...	$-4.670\ 80 \times 10^3$
φ	$-9.999\ 99 \times 10^{-1}$	$5.651\ 90 \times 10^{-8}$
η	$1.328\ 65 \times 10^{-7}$	4.701 63
τ	-7.498 08	$2.118\ 92 \times 10^{-7}$

tion mode theory,^{40,41} an attempt will be made in the following to formulate a conclusive answer using the finite element method.

A. Verification of validity of our model

For the first assumption, we will consider in the further paragraphs a combined analytical/numerical approach to confirm the transmission of the Rayleigh waves at the extremity of the solid plate. In the current paragraph, however, we try to obtain, in a first stage, the same result as shown in Fig. 9. To do this, we use a finite model in which the parameters are equal to the previously described one, except for the sonic frequency, the beam width, and the beam position. Here a 6 MHz Gaussian beam, moved towards the edge of the aluminum plate, having a physical width of $W \approx 7$ mm is used. The results obtained with the FEM are shown in Fig. 10. It is clear that the produced wave along the vertical edge, as seen in the real experiment (Fig. 9), is also found in the simulation. The additional null stripes along the vertical edge are made visible because of the use of a bilinear patterning curve to highlight the different waves in the finite element analysis: all the nodes of the fluid domain that have an intensity that is larger than a certain value are given the same intensity value. When this threshold value is taken rather low (as is the case here), these secondary null stripes become visible. The reason why they are not visible in the real experiment in Fig. 9 is that the schlieren technique cannot visualize such low pressure regions because of limited contrast.



B. Verification of assumption that leaky Rayleigh waves are stimulated by edge of the incident beam

For the second assumption, the question whether the outer parts of the bounded beam are responsible for the generation of the Rayleigh waves can be reformulated in the study of the influence of the Δ value on the generation of Rayleigh waves as in Ref. 1. The ability of different parts of a bounded beam to stimulate leaky Rayleigh waves can be expressed in terms of relative efficiency and must take into account the propagation distance between the spot of generation and the spot of detection. If, however, for smaller values of Δ , the intensity or a measure for the intensity of the generated Rayleigh waves turns out to be higher, one can conclude right away that the outer parts of the Gaussian beam are more efficient in generating Rayleigh waves and further investigations in terms of efficiency and distance become redundant. For this study, four finite element models, similar as the one used above, have been constructed, with the only mutual difference that they differ in the values of Δ , i.e., 0.2W, 0.4W, 0.8W, and 1.2W (complete incidence of the Gaussian beam on the solid plate), with $W \approx 7$ mm. For each of these configurations the directly incident power on the horizontal surface, i.e., the integration of (a measure of) the intensity along the fraction of the horizontal width W of the Gaussian beam on the horizontal surface of the solid plate, is measured. In the finite element simulations the square of the pressure in the fluid medium is taken as a measure of the intensity. The obvious result is found that more power is transferred directly to the solid plate in the 1.2W model than in the 0.8W model. This trend was also found for the 0.8W model compared with the 0.4W model and for the 0.4W model compared with the 0.2W model. To have an idea of the influence of the Δ on the generation of Rayleigh waves, the mean square of the acoustic pressure is measured along the lower part of the vertical edge of the solid plate. In Fig. 11, this measurement is plotted in function of the distance along the vertical edge. These graphs are very interesting though difficult to interpret because they represent a superposition of the different propagating waves in the solid and in the fluid medium. To make a comparison with the generation of Rayleigh waves possible, the lower part of the vertical edge of the solid plate has to be chosen in a way that the bulk waves propagating through the solid and the undis-

FIG. 13. (Color online) The transversal component of the Rayleigh wave in the x-y field.

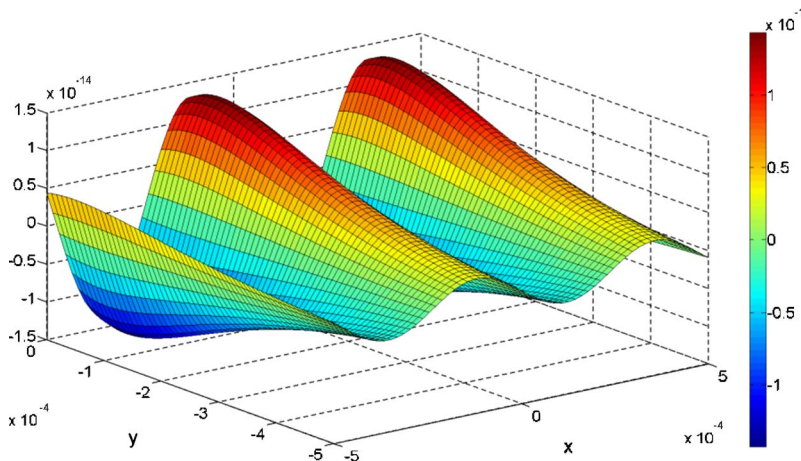


FIG. 14. (Color online) The longitudinal component of the Rayleigh wave in the x - y field.

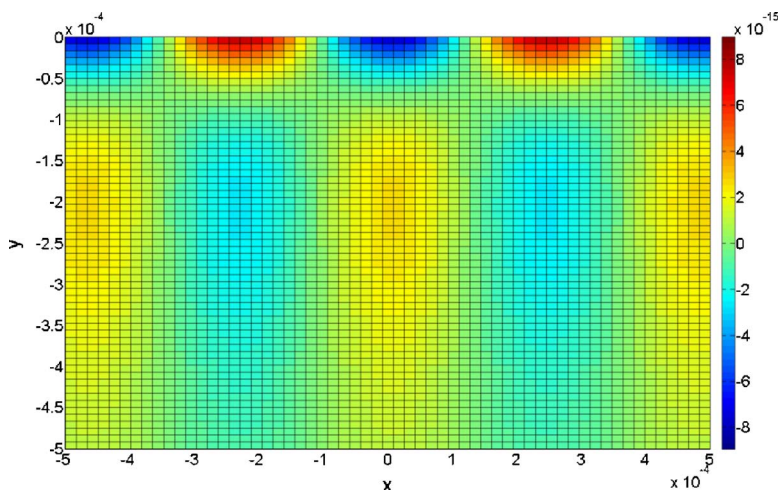


FIG. 15. (Color online) Top view of the transversal component of the Rayleigh wave.

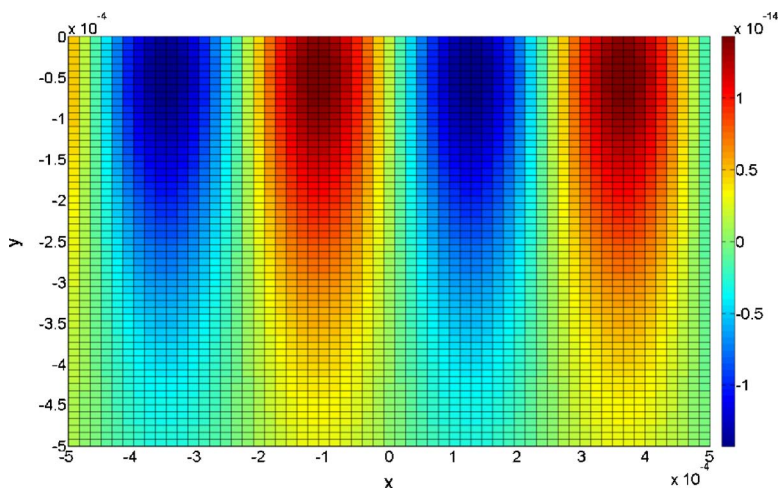


FIG. 16. (Color online) Top view of the longitudinal component of the Rayleigh wave.

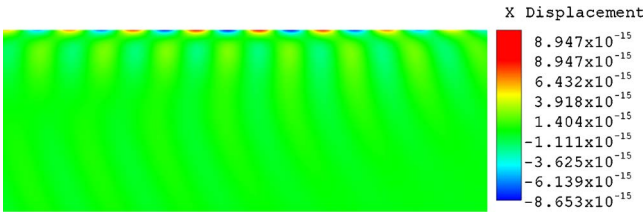


FIG. 17. (Color online) Simulation of the transversal displacement field in an aluminum plate caused by a 6 MHz incident Gaussian beam under the Rayleigh angle.

turbed incident waves may not influence the intensity in that specific region. This is shown in Fig. 12, where the mean square of the pressure is plotted along the interval [0.012m-0.0131m] on the vertical edge (far away from the zone where scattered waves are present). One can clearly see that the smaller the value for Δ becomes, the larger the intensity is. This confirms the indication given in Ref. 1 that the outer parts of the incident Gaussian beam are mainly responsible for the generation of the Rayleigh waves.

V. INTERNAL GENERATION OF RAYLEIGH WAVES

A. Combined analytical and numerical input

A firm proof that the Rayleigh waves travel around the corner must exclude all other phenomena as origins of the observed effects. A study of incident Rayleigh waves is therefore mandatory as it would exclude any influence of the incident bounded beam. Consideration of Rayleigh waves generated directly inside the solid material must investigate whether the Rayleigh waves themselves are responsible for the leakage of energy on the vertical side of the plate or not. Implementation of this problem in ABAQUS requires exact knowledge of the acoustic displacement fields inside the solid. The displacement fields are calculated by considering an ultrasonic plane wave, having the frequency we are interested in, incident from the liquid half space onto the interface between the liquid and the solid. Analytically (i.e., without any application of FEM) it is then possible to study the reflection coefficient for harmonic plane waves as well as the two transmission coefficients. The precise Rayleigh angle is found as the angle where the reflection coefficient shows a well-known phase shift⁴⁰ equals to π . The corresponding sound fields are then equally normalized and the ones inside the solid are used as boundary conditions in our FEM procedure. As a result we mathematically generate Rayleigh waves on the solid in our FEM program and we are able to study how these Rayleigh waves propagate along the inter-

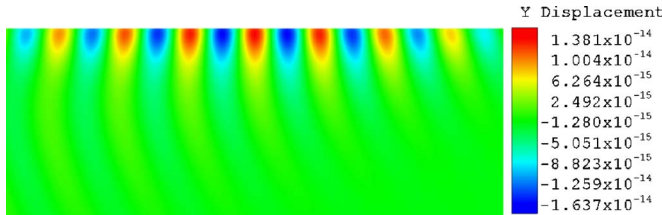


FIG. 18. (Color online) Simulation of the longitudinal displacement field in an aluminum plate caused by a 6 MHz incident Gaussian beam under the Rayleigh angle.



FIG. 19. Internal generation of the Rayleigh waves in an aluminum plate.

face and ultimately how they interact with the corner. The equations of motion of the induced Rayleigh waves in the solid material along the x and the y axes, according to the convention in Fig. 2, can be found in Eqs. (29) and (30), respectively. Their counterparts in the liquid are Eqs. (31) and (32).

For $y \leq 0$,

$$x_{\text{solid}} = (i\alpha\eta)e^{(i\alpha)x+(i\chi)y} - (i\epsilon\tau)e^{(i\alpha)x+(ie)y}, \quad (29)$$

$$y_{\text{solid}} = (i\chi\eta)e^{(i\alpha)x+(i\chi)y} + (i\alpha\tau)e^{(i\alpha)x+(ie)y}. \quad (30)$$

For $y > 0$,

$$x_{\text{liquid}} = (i\alpha\varphi\tau)e^{(ia)x+(i\beta)y}, \quad (31)$$

$$y_{\text{liquid}} = (i\beta\varphi\tau)e^{(ia)x+(i\beta)y}. \quad (32)$$

The constants α , β , χ , ϵ , φ , η , and τ that occur in the equations are bounded to the performed ultrasonic experiment and depend on the frequency of the beam, the fluid medium, the solid material, and the angle of incidence. The equation constants for this problem are given in their complex form in Table I.

If these constants are substituted into Eqs. (29) and (30), the longitudinal and the transversal motion equations of the Rayleigh waves in the solid material are obtained. The x - y field plot of these mathematical expressions can be found in Figs. 13 and 14. The top views of these plots are given in Figs. 15 and 16. The numerical longitudinal and transversal

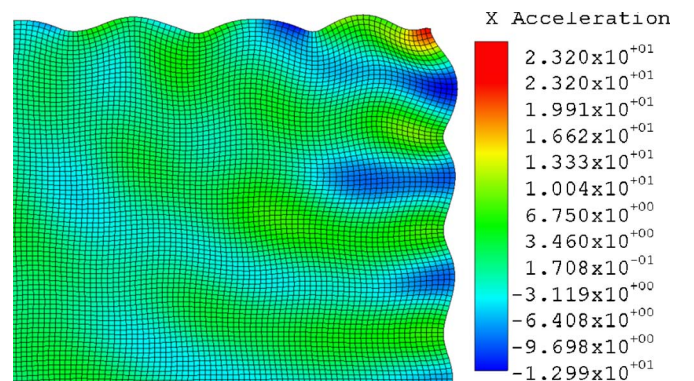


FIG. 20. (Color online) The spatial transversal acceleration in the nodes of an aluminum plate by an internal generated Rayleigh wave.

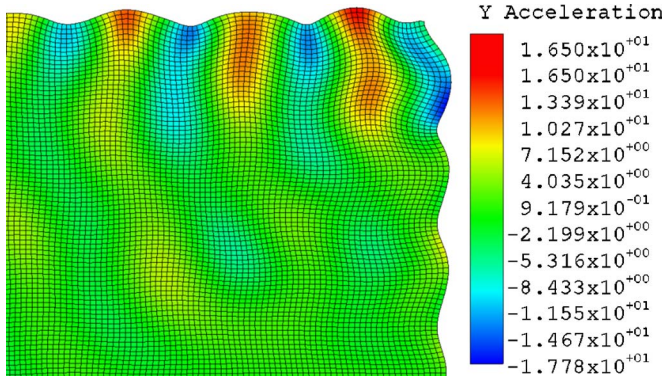


FIG. 21. (Color online) The spatial longitudinal acceleration in the nodes of an aluminum plate by an internal generated Rayleigh wave.

displacements field in ABAQUS for a 6 MHz ultrasonic incident Gaussian beam on a water-aluminum interface are shown in Figs. 17 and 18. One sees clearly the resemblance between the mathematically obtained plots (Figs. 15 and 16) and the finite element plots (Figs. 17 and 18). This means that the FEM enables fairly good simulation of the propagation of Rayleigh waves along the interface.

B. Numerical output

The internally generated Rayleigh waves in the aluminum plate are responsible for the ultrasonic waves at the solid-liquid interface. These waves, with a propagation direction that makes an angle of 31° with the vertical on the horizontal surface of the aluminum plate, can be observed in Fig. 19. In Figs. 20 and 21 we can see clearly that the elliptical Rayleigh acceleration of the surface nodes on the horizontal edge of the solid plate is passed on to the nodes of the vertical edge of the plate. This gives a decisive answer to the question whether Rayleigh waves travel around a corner of a solid plate. Further, it is also obvious that this elliptical Rayleigh movement on the vertical edge will leak energy in the fluid medium under the Rayleigh angle. Figure 19 shows that the produced waves in the fluid medium make again an angle of 31° with the horizontal.

VI. CONCLUSION

We investigated ultrasonic phenomena by application of the FEM. In order to prove the validity of the applied method, we simulated in ABAQUS the Schoch effect, which is a well-known ultrasonic phenomenon. After this, a next step has been set towards the simulation of an incident ultrasonic beam at the extremity of a solid plate. Agreement was found between numerical and experimental results. By combining a mathematical expression for the motion of the Rayleigh waves in the solid material and the FEM it was possible to show that leaky Rayleigh waves on the horizontal surface of the plate travel around the corner. These waves leak energy along the vertical part of the solid plate, which can be observed by the emission of waves in the liquid making the Rayleigh angle with the horizontal.

In addition evidence was found for the assumption that leaky Rayleigh waves are primarily generated by the edge of an incident bounded beam, rather than by the middle.

ACKNOWLEDGMENT

The authors gratefully acknowledge financial support for this research by the Fund for Scientific Research-Flanders (FWO).

- ¹N. F. Declercq, A. Teklu, M. A. Breazeale, R. Briers, O. Leroy, J. Degrieck, and G. N. Shkerdin, *J. Appl. Phys.* **96**, 5836 (2004).
- ²M. A. Breazeale, L. Adler, and G. W. Scott, *J. Appl. Phys.* **48**, 530 (1977).
- ³J. M. Claeys and O. Leroy, *J. Acoust. Soc. Am.* **72**, 585 (1982).
- ⁴M. Debilly and I. Molinero, *J. Acoust. Soc. Am.* **83**, 1249 (1988).
- ⁵T. Kundu, *J. Acoust. Soc. Am.* **83**, 18 (1988).
- ⁶W. G. Neubauer, *J. Appl. Phys.* **44**, 48 (1973).
- ⁷T. D. K. Ngoc and W. G. Mayer, *J. Acoust. Soc. Am.* **67**, 1149 (1980).
- ⁸J. Pott and J. G. Harris, *J. Acoust. Soc. Am.* **76**, 1829 (1984).
- ⁹A. B. Temsamani, S. Vandenplas, and L. Van Biesen, *Ultrasonics* **38**, 749 (2000).
- ¹⁰W. G. Neubauer and L. R. Dragonet, *J. Appl. Phys.* **45**, 618 (1974).
- ¹¹A. L. Araujo, C. M. M. Soares, J. Herskovits, and P. Pedersen, *Compos. Struct.* **58**, 307 (2002).
- ¹²Z. Y. Jiang, S. W. Xiong, X. H. Liu, G. D. Wang, and Q. Zhang, *J. Mater. Process. Technol.* **79**, 109 (1998).
- ¹³X. K. Li, Z. J. Liu, and R. W. Lewis, *Int. J. Numer. Methods Eng.* **64**, 667 (2005).
- ¹⁴T. Matsuoka, S. Yamamoto, and M. Takahara, *J. Mater. Sci.* **36**, 27 (2001).
- ¹⁵H. F. Tan, X. W. Du, Y. T. Wei, and Y. J. Yum, *Veh. Syst. Dyn.* **40**, 161 (2003).
- ¹⁶K. Weide, X. Yu, and F. Menhorn, *Microelectron. Reliab.* **36**, 1703 (1996).
- ¹⁷T. Zeng, L. Z. Wu, and L. C. Guo, *Compos. Struct.* **64**, 399 (2004).
- ¹⁸L. F. Guo, T. M. Yue, and H. C. Man, *J. Laser Appl.* **16**, 229 (2004).
- ¹⁹Y. Islamoglu, *Mater. Des.* **25**, 479 (2004).
- ²⁰Z. Y. Jiang, A. K. Tieu, C. Lu, W. H. Sun, X. M. Zhang, X. H. Liu, G. D. Wang, and X. L. Zhao, *Finite Elem. Anal. Design* **40**, 1139 (2004).
- ²¹T. Kant and C. S. Babu, *Compos. Struct.* **49**, 77 (2000).
- ²²S. P. Kovalev, P. Miranzo, and M. I. Osendi, *J. Am. Ceram. Soc.* **81**, 2342 (1998).
- ²³A. P. Bagshaw *et al.*, *Neuroimage* **20**, 752 (2003).
- ²⁴J. L. Guermond, J. Leorat, and C. Nore, *Eur. J. Mech. B/Fluids* **22**, 555 (2003).
- ²⁵E. J. Woo, P. Hua, J. G. Webster, and W. J. Tompkins, *Med. Biol. Eng. Comput.* **32**, 530 (1994).
- ²⁶Z. Y. Zhu, H. P. Lee, and B. T. Cheok, *J. Electron. Packag.* **125**, 144 (2003).
- ²⁷C. Campos-Pozuelo, B. Dubus, and J. A. Gallego-Juarez, *J. Acoust. Soc. Am.* **106**, 91 (1999).
- ²⁸A. C. Hladky-Hennion, P. Langlet, and M. de Billy, *J. Sound Vib.* **200**, 519 (1997).
- ²⁹T. F. Johansen, J. F. Allard, and B. Brouard, *Acta Acust.* **3**, 487 (1995).
- ³⁰M. Koshiba, S. Karakida, and M. Suzuki, *IEEE Trans. Sonics Ultrason.* **31**, 18 (1984).
- ³¹F. Treyssede, G. Gabard, and M. Ben Tahar, *J. Acoust. Soc. Am.* **113**, 705 (2003).
- ³²B. Q. Xu, Z. H. Shen, X. W. Ni, J. Lu, and Y. W. Wang, *J. Appl. Phys.* **95**, 2109 (2004).
- ³³R. J. Bernhard and J. E. Huff, *Trans. ASME, J. Vib. Acoust.* **121**, 295 (1999).
- ³⁴J. R. Cho, H. W. Lee, and K. W. Kim, *J. Sound Vib.* **258**, 847 (2002).
- ³⁵G. C. Everstine, *Comput. Struct.* **65**, 307 (1997).
- ³⁶Y. J. Kang and J. S. Bolton, *J. Acoust. Soc. Am.* **98**, 635 (1995).
- ³⁷A. Mar-Or and D. Givoli, *J. Comput. Acoust.* **12**, 605 (2004).
- ³⁸A. Schoch, *Acustica* **2**, 18 (1952).
- ³⁹A. Schoch, *Acustica* **2**, 1 (1952).
- ⁴⁰N. F. Declercq, Ph.D. thesis, Ghent University, 2005.
- ⁴¹N. F. Declercq, R. Briers, O. Leroy, J. Degrieck, and G. N. Shkerdin, *IEEE Trans. Ultrason. Ferroelectr. Freq. Control* **52**, 802 (2005).